Emission Control Science and Technology (2019) 5:263–278
https://doi.org/10.1007/s40825-019-00127-0

Selective Catalytic Reduction of NO_x over V_2O_5-WO_3-TiO_2 SCR Catalysts—A Study at Elevated Pressure for Maritime Pre-turbine SCR Configuration

Steen R. Christensen[1] · Brian B. Hansen[1] · Kim H. Pedersen[2] · Joakim R. Thøgersen[2] · Anker D. Jensen[1]

Received: 10 April 2019 / Revised: 11 June 2019 / Accepted: 27 June 2019 / Published online: 4 July 2019

Abstract

The selective catalytic reduction (SCR) of NO_x using NH_3 was studied at pressures up to 5 bar over a vanadium-based SCR catalyst (~1 wt% V_2O_5 and 10 wt% WO_3/TiO_2), relevant for the installation of SCR reactors upstream of the turbocharger at marine engines. Experiments were performed using both granulated catalyst in a lab-scale fixed-bed reactor and a monolith catalyst in a bench-scale setup. The residence time across the catalytic bed was kept constant, by increasing the (normalized (0 °C, 1 atm)) volumetric flow rate proportionally to the pressure. The results show that for the granulated catalyst, the NO_x conversion was independent of the pressure, indicating that the SCR kinetics are not affected by the increased pressure up to 5 bar. NH_3 temperature-programmed desorption experiments showed that the catalyst NH_3 adsorption increased with more than 30% when the pressure was increased from 1 bar to 4.5 bar. On the other hand, when the adsorption temperature was increased from 150 to 300 °C, the adsorption capacity decreased by approximately 60% independent on the pressure. The SCR reaction was unaffected by the increased NH_3 uptake caused by the increased pressure, because only a certain fraction of the sites ($\theta^*_{NH_3} = 0.14$) was found to be active in the SCR reaction, and these are filled up at lower NH_3 partial pressure than the total number of sites. Experiments using a monolithic catalyst showed that at temperatures above 250 °C, the NO_x conversion was lower at an increased pressure (3.1 bar) when the residence time was held constant. This decrease was ascribed to increased internal and external diffusion limitations at the elevated pressure.

Keywords Pre-turbo SCR · SCR of NO_x on ships · High-pressure SCR of NO_x · NH_3 TPD · *V*/*W*/Ti catalyst

1 Introduction

Currently, more than 80% of the international transport of goods is covered by ships [1, 2], and the majority of these (> 90% [3]), are powered by diesel engines. The diesel engine benefits from low emissions of CO_2 (g/km); however, pollutants causing acidification and smog such as SO_x (SO_2, SO_3, and H_2SO_4) and NO_x (NO and NO_2) are produced [4–8]. It has been estimated that approximately 30% of the global anthropogenic NO_x emissions originate from the overall transport sector, and 5–15% originate from the marine industry alone [4, 9]. The emissions of NO_x and SO_x are therefore targeted by the emission legislation presented by the international maritime organization (IMO) through the protocol of MARPOL 73/78 Annex VI [10].

SO_x emissions are produced due to the sulfur content of the fuel oil used at a ship, and MARPOL Annex VI regulation 14 therefore limits the fuel oil sulfur content to 3.5 wt% until 2020 [11], after which the global value is further reduced to 0.5 wt% sulfur in the fuel oil or an equivalent treatment of the exhaust gas. Furthermore, since 2015 when sailing within SO_x emission control areas (SECAs), the sulfur emissions from a ship must be equivalent to using a fuel oil containing no more than 0.1 wt% sulfur. The currently known SECAs are the Baltic Sea, the North Sea, the North American sea area, and the US Caribbean Sea area [12].

NO_x emissions are produced in high-temperature combustion zones within the combustion chamber, mainly through the Zeldovich mechanism, independent of the fuel oil used [13, 14]. NO is the main contributor (> 90%) to the NO_x emissions from diesel engines [15–19].

Electronic supplementary material The online version of this article (https://doi.org/10.1007/s40825-019-00127-0) contains supplementary material, which is available to authorized users.

✉ Anker D. Jensen
aj@kt.dtu.dk

[1] Department of Chemical and Biochemical Engineering, Technical University of Denmark, Søltofts Plads B229, 2800 Kgs. Lyngby, Denmark

[2] Umicore Denmark ApS, Nøjsomhedsvej 20, 2800 Kgs. Lyngby, Denmark

NO_x emissions are targeted through the introduction of MARPOL Annex VI, regulation 13, Tier I (2000) and Tier II (2011), both of which were reachable by the use of primary methods which reduces the combustion temperature, and therefore, also the production of NO_x. With the introduction of MARPOL Annex VI Tier III (2016), 80% NO_x reduction is required compared to the Tier I regulation. Tier III applies to all ships constructed after 2016 and when sailing within NO_x emission control areas (NECAs), which currently is the North American sea area and the US Caribbean Sea area [12].

The two leading global engine manufacturers, MAN Energy Solutions and Wärtsilä, have stated that multiple solutions exist to comply with the new NO_x regulation. At the moment, the most favorable solutions are the use of either exhaust gas recirculation (EGR) [3, 20], selective catalytic reduction (SCR) of NO_x, or dual-fuel engines fueled by either conventional liquid marine fuels or liquid natural gas (LNG) [21]. In this article, the focus will be on the SCR of NO_x.

SCR of NO_x was first introduced in the 1970s and 1980s for the removal of NO_x from stationary applications such as power plants, waste incinerators, and within the chemical industry [15, 22, 23]. NO_x is typically reduced over a catalyst containing 1–5 wt% V_2O_5/~10 wt% WO_3/TiO_2 (V-SCR catalyst) using an N-containing reductant such as ammonia (NH_3) on stationary units or an aqueous urea solution on mobile units, which decomposes into NH_3 upon heating [15, 16, 24, 25]. The SCR of NO_x typically proceeds at temperatures between 200 and 500 °C, during which NO is reduced according to reaction (1) into harmless nitrogen and water. Depending on the applied ammonia to NO_x ratio (ANR), NO_x reductions above 90% is reachable.

$$4\ NO + 4\ NH_3 + O_2 \rightarrow 4\ N_2 + 6\ H_2O \tag{1}$$

A highs sulfur fuel oil (approx. 2.5 wt% sulfur [26]) is typically used within the marine industry, which results in concentrations of up to 600 ppm SO_2 in the flue gas. Up to 10% of the SO_2 is further oxidized into SO_3 within the combustion chamber [27], and a small part of the remaining SO_2 (1–3% [28, 29]) is oxidized across the V-SCR catalyst according to reaction (2). The V-SCR catalyst is not deactivated by the presence of SO_2; however, when both SO_3, H_2O, and NH_3 are present in the exhaust gas, ammonium bisulfate (ABS, reaction (3)), and ammonium sulfate (AS, reaction (4)) may form when the exhaust gas is cooled [30–32].

$$SO_2 + {}^1/_2\ O_2 \rightarrow SO_3 \tag{2}$$

$$NH_3 + SO_3 + H_2O \rightarrow NH_4HSO_4 \tag{3}$$

$$2\ NH_3 + SO_3 + H_2O \rightarrow (NH_4)_2SO_4 \tag{4}$$

The sulfates condense, creating solid residues, at temperatures below 260–300 °C, depending on the partial pressures of NH_3 and SO_3. If the sulfates condense at the surface or within the pores of the catalyst [30], the catalyst is deactivated by the fouling, and hence, temperatures higher than about 300 °C are required in order to keep the catalyst active in high sulfur environments, such as a ship. For the highly effective two-stroke marine diesel engine, such high temperatures are only continuously present upstream of the turbocharger, where an increased pressure of up to 5 bar also can be present depending on the engine load [20, 33–38].

The research within SCR at elevated pressure is scarce and only a few previous studies have been published. Kröcher et al. [35] measured the effect of increased pressure on NO_x conversion over two monolith V-SCR catalysts (1.47 wt% V_2O_5) with either 87 or 225 channels per square inch (CPSI). The experiments were performed with 1000 ppm NO_x, ANR > 1, at pressures of 1 bar, 2 bar, and 4 bar. They kept the partial pressure of NO and NH_3 constant, and decreased the amount of catalyst inversely proportional to the pressure, so the actual gas residence time was independent of the reaction pressure. They noted that at low temperature (200 °C), the pressure had no effect on the NO_x conversion. However, at higher temperatures (> 250 °C), increased pressure resulted in a lower NO_x conversion, from 70% at 1 bar to 50% at 4 bar at 250 °C using the 225 CPSI catalyst. The loss in NO_x conversion was attributed to increased diffusion limitations, due to the inverse proportionality between pressure and the binary diffusion coefficient [39].

Rammelt et al. [36] also investigated the effects of increased pressure on two V-SCR (1.9 wt% V_2O_5) monolith catalysts with either 300 or 25 CPSI. In line with Kröcher et al. [35], they observed a drop in NO_x conversion with increasing pressure which was more pronounced for the low CPSI catalyst, due to longer diffusion pathways.

The present study investigates SCR at elevated pressure, using both lab-scale packed bed reactors and bench-scale monoliths to test the effects of pressure on SCR kinetics. Furthermore, the transient adsorption and desorption of NH_3 at increased pressures up to 4.5 bar are investigated to reveal information of the changes in NH_3 adsorption with pressure. Based on the experiments, both steady-state SCR kinetics and dynamic adsorption and desorption processes are modeled. The side reaction of SO_2 oxidation was studied in a previous publication by Christensen et al. [40].

2 Experimental Methods

2.1 Lab-Scale Setup

2.1.1 Apparatus

The packed bed reactor shown schematically in Fig. 1 was used for kinetic SCR studies up to 5 bar. Four mass flow controllers from Brooks (SLA5850) controlled the gas

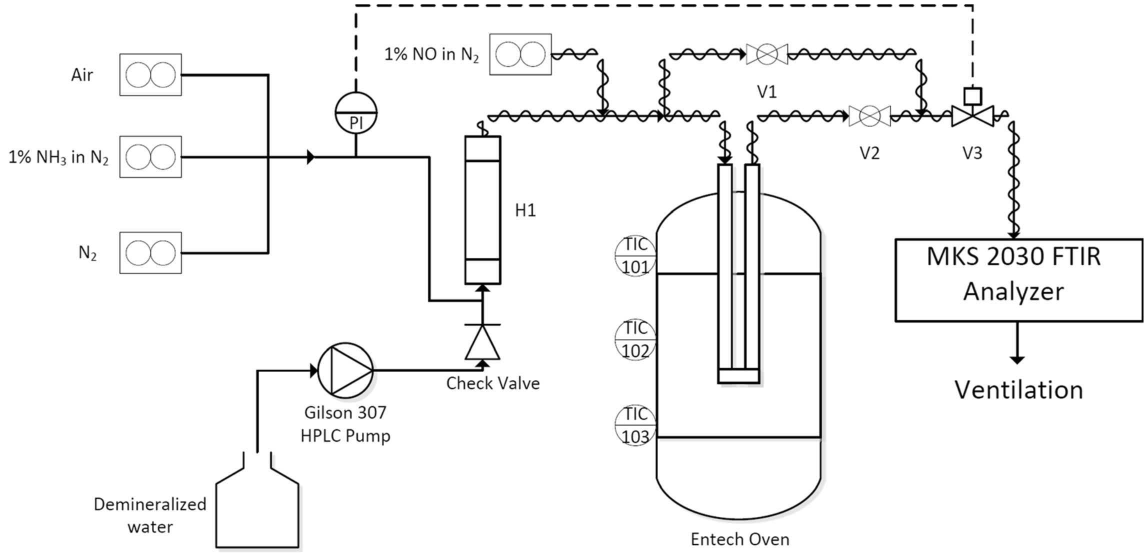

Fig. 1 The lab-scale test setup used for SCR experiments and NH_3 TPD experiments at elevated pressure using a granulated V-SCR catalyst

composition. Water was added by the use of a HPLC pump (Gilson 307) and carried together with air, nitrogen, and ammonia into the homemade evaporator (H1), which consisted of 0.5 m 1/8 in 316 steel tube which was coiled together with heat tracing (HSS from Lund & Sørensen) and operated at a temperature of 350 °C. After the evaporator, all tubes were heat traced to 150 °C to ensure that water vapor did not condense. NO was added to the hot gas downstream of the evaporator, to ensure that the oxidation of NO into NO_2 was low, similar to diesel engine conditions ($NO > 90\%\ NO_x$ [41]).

The synthetic gas mixture was passed through a packed bed reactor, contained within a U-type quartz reactor. The position of the catalytic bed was maintained by a quartz wool plug on both sides, and a constriction of the glass tube, beneath the catalyst bed. A thermocouple was placed before the catalytic bed, to measure the temperature. After the reactor, the pressure was reduced by two automatic back pressure valves (Fisher Fieldvue DVC 2000), and gas concentrations were measured at atmospheric pressure using an MKS Multigas 2030 FTIR analyzer.

2.1.2 Catalyst

An SCR catalyst containing approximately 1 wt% V_2O_5/10 wt% WO_3/TiO_2 (V-SCR) was supplied by Umicore Denmark ApS. The catalyst was produced as a monolith, from which the catalyst powder was obtained by crushing and removing of visible fibers. The powder was pressed into self-supporting pellets, which were crushed and sieved into catalyst particles with a size fraction of 150–300 μm, and loaded in the reactor setup. The fraction of 150–300 μm was chosen to diminish diffusion limitations, as shown in the online supplementary material..

2.1.3 Steady-State SCR—Experimental Methodology

Approximately 20 mg of catalyst was loaded in a U-type quartz reactor (as shown in Fig. 2a) with an inner diameter of 3 mm, resulting in a bed height of 4 mm. Catalysts were degreened for 20 hours at 410 °C and 4.8 bar using a volumetric flow rate of 1200 NmL/min, containing 10% O_2, 8% H_2O, 600 ppm NO_x, and 720 ppm NH_3 in N_2.

After degreening, steady-state SCR experiments were carried out with typical gas concentrations of 10% O_2, 8% H_2O, 600 ppm NO_x, and an ammonia to NO_x ratio (ANR) of 0.8–1.2 in N_2. The pressure was varied in steps of 1.2 bar up to 4.8 bar. The residence time within the catalyst bed was kept independent of pressure by increasing the total volumetric flow rate proportional with the pressure as shown in Eq. (5):

$$Q_{total@P} = Q_0 \cdot \frac{P_{reactor}}{1\text{atm}} \tag{5}$$

Here, Q_0 is the design total volumetric flow rate (normal (0 °C, 1 atm)) used at 1 atm, $P_{reactor}$ is the reactor pressure, and $Q_{total@P}$ is the total volumetric flow rate calculated for the specific pressure. At 1.2 bar, a total volumetric flow rate of 300 NmL/min was used and at 4.8 bar a total volumetric flow rate of 1200 NmL/min was used. The gas outlet concentrations were continuously measured by the FTIR analyzer using the mean results of 16 spectra per sample resulting in gas concentration outputs every 16th second.

2.1.4 NH_3 TPD—Experimental Methodology

Approximately 115 mg of catalyst loaded in a U-type quartz reactor, with an inner diameter of 4 mm. The catalyst was degreened for 20 hours at 410 °C and 4.5 bar using a total

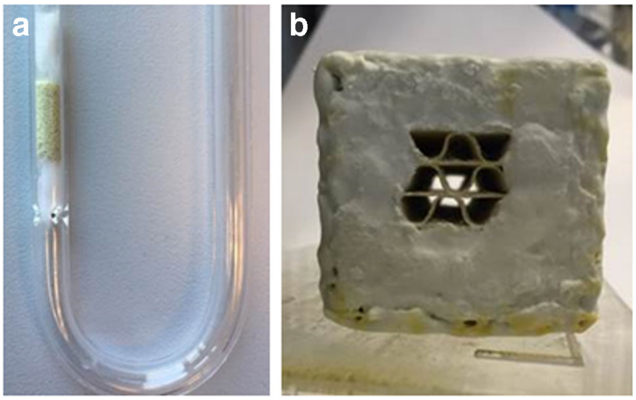

Fig. 2 Granulated catalyst particles in a packed bed reactor (PBR) (**a**) and the monolith catalyst with nine open channels (**b**)

volumetric flow rate of 600 NmL/min containing 9% O_2, 8% H_2O in N_2. The increased reactor diameter was used to decrease the pressure drop over the increased amount of catalyst, compared to the steady-state SCR experiments.

The NH_3 temperature programmed desorption (NH_3 TPD) experiments consisted of 1 hour of NH_3 adsorption at a specific temperature (150 °C, 200 °C, 250 °C, and 300 °C) and pressure using a flow of 300 NmL/min containing 9% O_2, 8% H_2O, and 600 ppm NH_3 in N_2. During NH_3 TPD experiments, the total volumetric flow rate was kept constant at 300 NmL/min. After 1 hour, the outlet concentration of NH_3 was the same as the inlet concentration (typically already after 5-10 min.), i.e., the catalyst surface was saturated, and the flow of NH_3 and H_2O was stopped. Feeding of H_2O was stopped to remove small pulsations from the pumping and evaporation of H_2O, so the desorption curve was smooth. During desorption, a total volumetric flow rate of 300 NmL/min was used at 1 bar, while in all other experiments, a total volumetric flow rate of 276 NmL/min was used due to slightly different set points of the nitrogen MFC setting. After flushing for 1 hour, a temperature ramp (10 K/min) was performed from the saturation temperature and until 420 °C. The temperature was maintained at 420 °C for 20 min before the reactor was cooled to the next adsorption temperature. The gas outlet concentrations were continuously measured by the FTIR analyzer using the mean of two spectra per sample resulting in gas concentration outputs every 2 s.

During NH_3 adsorption, the outlet concentration was observed to correspond to the inlet concentration indicating that no NH_3 oxidation was present at any adsorption temperatures (150–300 °C). Ammonia oxidation could occur under the desorption; however, for the applied low vanadium-based catalyst, NH_3 oxidation is first expected at temperatures well above 350 °C, during which most of the NH_3 has been desorbed. Therefore, NH_3 oxidation has been disregarded.

Blank experiments (i.e., no catalyst loaded) were performed to examine the response of the setup when NH_3 addition was stopped. The first blank experiment was performed at 1.2 bar, with NH_3 adsorption steps at 150 °C, 200 °C, 250 °C, and 300 °C all followed by the described heating ramp. However, since no change was observed between the different temperatures, the ramp was skipped, and the blank experiments were performed without the ramp to save time and only at a temperature of 150 °C. Because the ramp was skipped, the blank experiments were shorter than the actual experiment.

2.2 Bench-Scale Setup

2.2.1 Apparatus

Experiments using monolith catalyst elements at elevated pressure were performed with the setup previously described in detail, for the measurements of pressurized SO_2 oxidation over a V-SCR catalyst by Christensen et al. [40]. The setup is a bench-scale setup for testing monolith catalysts using Brooks smart flow controllers for gasses (Air, N_2, NO, and NH_3) and Brooks liquid mass flow controller (model 5882) for water addition. Air, nitrogen, and water were passed through a preheater, in which water was evaporated. The gas mixture was further heated in a second heater, after which NH_3 and NO were added upstream of a static mixer from Sulzer, from which the hot mixed gas was passed through the monolith catalyst. The catalyst was placed within a square electrically heated furnace, and gas analysis was performed using a Gasmet FTIR analyzer (GASMET DX - 4000) by the withdrawal of gas before and after the catalyst.

2.2.2 Catalyst

A V-SCR monolith catalyst (~1 wt% V_2O_5/10 wt% WO_3/TiO_2) was cut into a square cross-sectional area (43.5 mm), and a length of 99.1 mm and the sides were sealed with quartz wool. Furthermore, to reduce external mass transfer limitations and the NO_x conversion, all but nine channels of the monolith were sealed resulting in an open area of 223 mm^2, i.e., area without the channel walls, as shown in Fig. 2b.

2.2.3 Steady-State SCR—Experimental Methodology

The monolith was loaded into the reactor setup, and the catalyst was degreened at 410 °C in a flow of air and 5% H_2O for 15 hours. The SCR reaction was performed at 1 and 3 bar while keeping the residence time independent of the pressure as shown in Eq. (5). At 1 bar, a flow of 4.9 Nm^3/h was used containing 8% O_2, 5% H_2O, 720 ppm NO_x, and ANR = 0.75 or 1.16 in N_2.

3 Results

3.1 High-Pressure Steady-State SCR Experiments

The SCR experiments were carried out at steady-state conditions, and the measured NO_x conversion as a function of temperature is shown for ANR = 1.2 and ANR = 0.8 in Fig. 3.

Figure 3 shows that the NO_x conversion is independent of the pressure when the residence time is kept constant. The NH_3 and NO_x consumption was found to follow the stoichiometry according to reaction (1) (1:1), within 5% of the total NO_x concentration, or at low concentration (< 100 ppm) where differences in gas measurements give a large error within 15 ppm. Formation of other byproducts such as N_2O from NH_3 oxidation was not observed at any conditions. At atmospheric pressure water is known to limit the formation of N_2O across V-SCR due to competitive adsorption [7, 24], which also seems to apply for increased pressure. Figure 3 shows that the kinetics of the SCR reaction is not affected by pressures up to 4.8 bar. The small variations observed are within the experimental uncertainty. Furthermore, Fig. 3b shows that when NH_3 becomes the limiting reactant at high temperatures, the conversion of NO_x levels off at a NO_x conversion close to the ANR value, as also typically reported for atmospheric pressures. The fact that the SCR reaction is not affected by the increased pressure also means that a regular kinetic expression [15, 24, 42, 43] taking into account the NH_3 surface coverage can be used, either in more complicated forms of Temkin isotherms as discussed later or using regular Langmuir isotherms as in the simplified Eley-Rideal mechanism [42] as given in Eq. (6). Figure 3a also indicates that the reaction can be treated as a first-order reaction at ANR > 1, because the conversion does not change when the pressure is increased, i.e., no changes at increased partial pressures.

$$R_{NO} = k_{NO} \cdot C_{NO} \frac{K_{NH_3} \cdot C_{NH_3}}{1 + K_{NH_3} \cdot C_{NH_3}} \tag{6}$$

The addition of NO to the hot gas ensured that the maximum concentration of NO_2 in the feed gas was 40 ppm NO_2 (at 4.8 bar) out of a total NO_x concentration of 600 ppm, which was not observed to change the NO_x reduction, so the reaction can be modeled as only the standard SCR reaction, i.e., considering all NO_x as NO.

To investigate the NO reaction order, inlet NO concentrations of 300, 600, and 900 ppm NO were used, with constant residence time and using an ANR of 0.8 or 1.2 as shown in Fig. 4.

Figure 4 shows that changing the inlet NO_x concentration from 600 to 900 ppm did not affect the NO_x conversion as expected for a reaction that is first order in NO. The NO_2 concentration increased to 50 ppm for the case of 900 ppm NO_x at 3.6 bar, i.e., 94% of NO_x is NO, and the assumption of only standard SCR is still applicable. When the inlet NO_x concentration was lowered to 300 ppm (at 3.6 bar), the NO_x conversion unexpectedly increased at the lower temperature range which is expected to be due to an unintended increased residence time within the catalyst. A concentration of 300 ppm of NO_x is well within normal atmospheric SCR operation [24, 44]. The expected effects of increased pressure include increased NH_3 adsorption, decreased diffusivity, and the possibility of increased formation of NO_2. The increased NH_3 adsorption at increased pressure should not affect an experiment with ANR = 1.2, because the rate of NO reaction

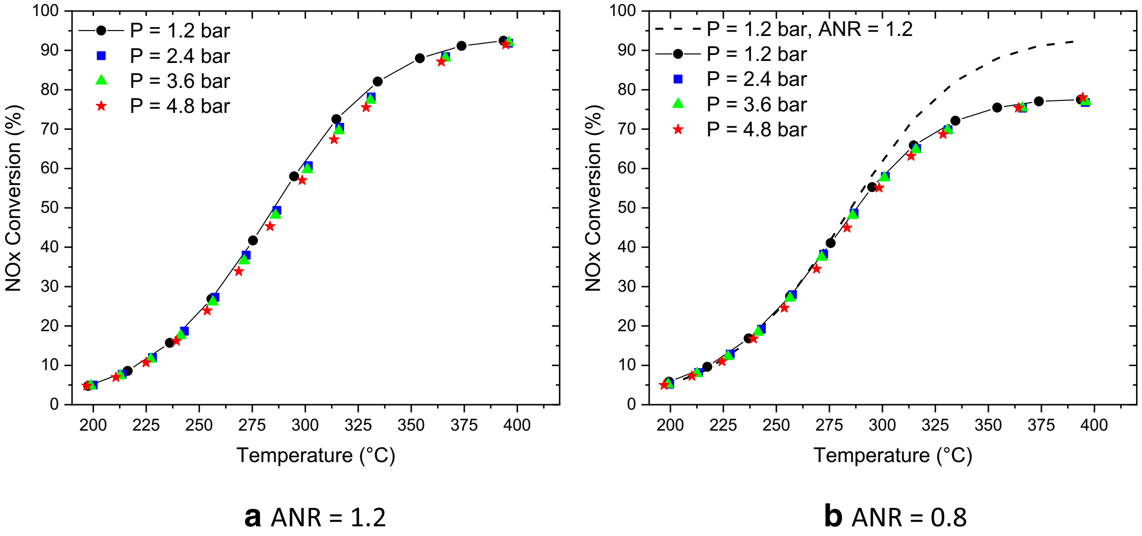

a ANR = 1.2 **b** ANR = 0.8

Fig. 3 Packed bed steady-state SCR experiments using 20.8 mg (~1 wt% V_2O_5) V-SCR catalyst and a flow of 300 NmL/min at 1.2 bar containing 10% O_2, 8% H_2O, 600 ppm NO_x, ANR = 1.2 (**a**), or ANR = 0.8 (**b**) in N_2. The residence time was kept constant by increasing the total volumetric flow rate according to Eq. (5)

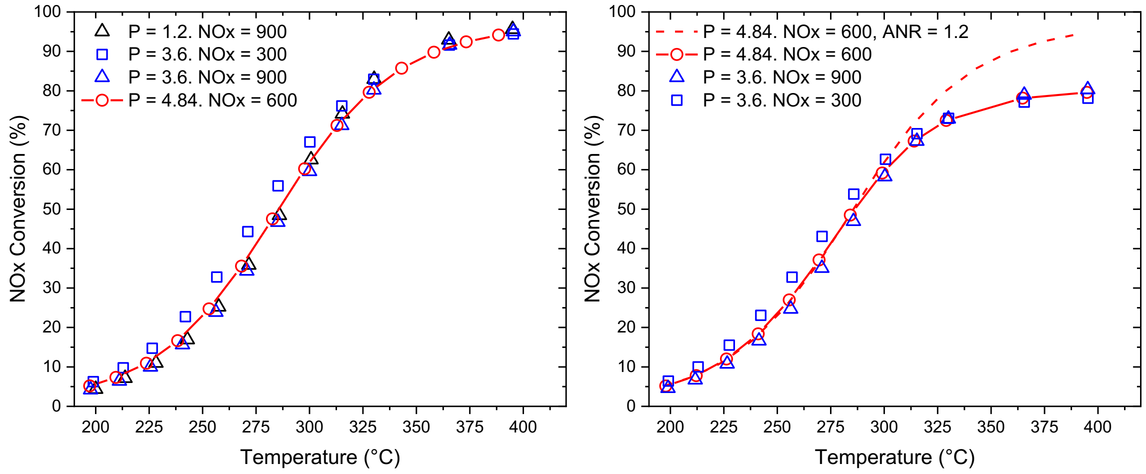

a ANR = 1.2

b ANR = 0.8

Fig. 4 Packed bed steady-state SCR experiments using 20.5 mg (~1 wt% V_2O_5) V-SCR catalyst and a flow rate of 300 NmL/min at 1.2 bar containing 10% O_2, 5% H_2O, 300, 600, or 900 ppm NO_x, ANR = 1.2 (**a**) or ANR = 0.8 (**b**) in N_2. The residence time was kept constant by increasing the total volumetric flow rate according to Eq. (5)

is independent of NH_3 coverage, as also will be shown later. Furthermore, the behavior should have been visible independently of the NO_x inlet concentration. A decrease in diffusivity would lower the NO_x conversion and is first observed in diffusion-controlled operation, such as a monolith, and again should be present independently of the NO_x inlet concentration. Lastly, the increased formation of NO_2 at increased pressure was observed, however, never exceeding 6% of the total NO_x and the effect is more pronounced at increased NO_x concentrations due to a second-order reaction dependency in NO for the NO oxidation [45]. Therefore, the change in conversion observed with an inlet concentration of 300 ppm NO_x at an ANR of 1.2 or 0.8 is likely due to an unintended lower total volumetric flow rate, resulting in increased residence time.

3.2 NH_3 TPD at Elevated Pressure

NH_3 TPD experiments were performed at 1.2, 2.4, 3.6, and 4.5 bar using a total volumetric flow rate during adsorption of 300 NmL/min containing 9% O_2, 8% H_2O, and 600 ppm NH_3 in N_2. A typical set of data for TPD at 1.2 bar is shown in Fig. 5. Similar plots for 2.4, 3.6, and 4.5 bar and a zoom of the NH_3 peaks can be found in the online supplementary material.

Figure 5 shows that loosely bound NH_3 desorbs during the 1-hour flush, while the rest of the NH_3 is released during the temperature ramp. No NH_3 was released during the 20-min isotherm at 420 °C. Integration of the data for the desorption of NH_3 was performed at each pressure and temperature, to calculate the amount of NH_3 adsorbed on the surface of the catalyst. Integration of the full desorption curve was performed, but also the heating ramp peak only. The blank experiments, performed without a catalyst, resulted in full desorption backgrounds of 97, 150, 166, and 166 μmol/g_{cat} NH_3 at 150 °C, and a pressure of 1.2, 2.4, 3.6, and 4.5 bar, respectively. The background integration was divided by the amount of catalyst used in the actual experiments, to ease comparison. The backgrounds were withdrawn from the integration, and the NH_3 adsorbed on the surface of the catalyst was calculated as shown in Fig. 6.

Figure 6 shows that in general the ammonia, adsorption increases as the pressure increases, and that the ammonia adsorption decreases as the adsorption temperature increases. Figure 6a shows that at the high adsorption temperature of 300 °C, the adsorption capacity of the catalyst is similar at pressures above 2.4 bar. At this high temperature, the amount of NH_3 stored on the catalyst is low, and hence, the small increase, at increased pressure, is likely hidden within the uncertainty (± 5% of the mean) of the blank experiments.

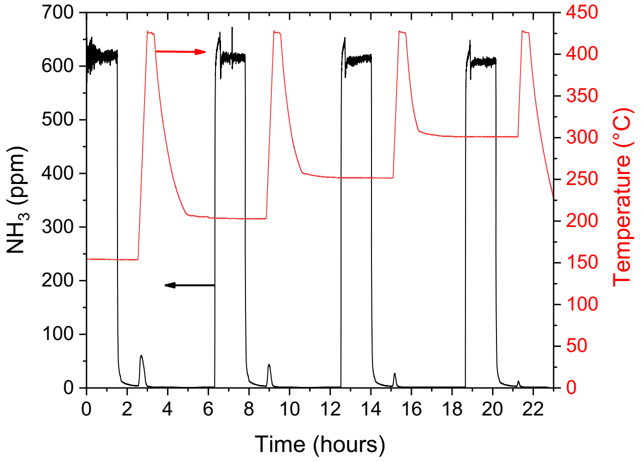

Fig. 5 NH_3 TPD at a pressure of 1.2 bar. NH_3 adsorption is performed at four different temperatures (150, 200, 250, and 300 °C), using a total volumetric flow rate during adsorption of 300 NmL/min containing 9% O_2, 8% H_2O, and ~600 ppm NH_3 in N_2

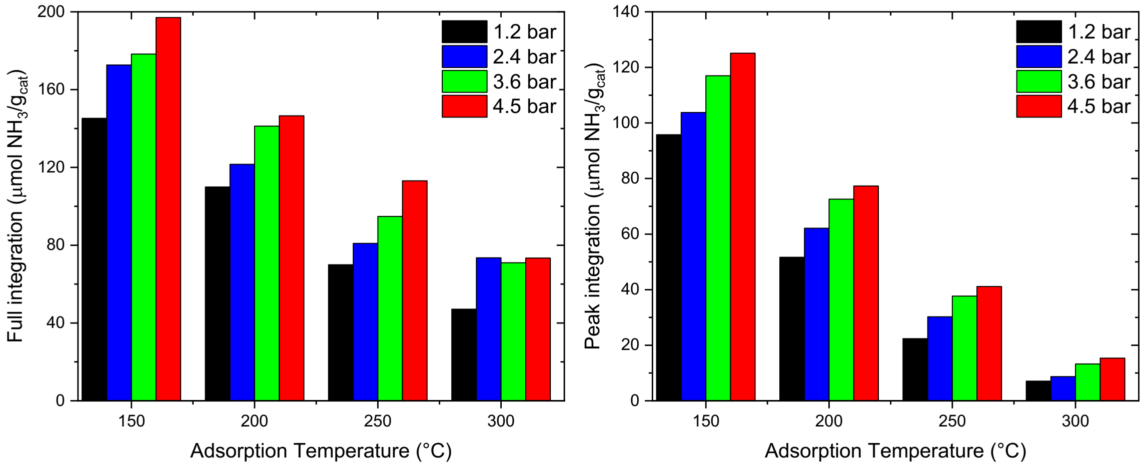

a Integration of the full desorption trace of NH3

b Integration of the desorption peak

Fig. 6 The amount (μmol NH_3/g_{cat}) of NH_3 adsorbed on the catalyst for the full desorption curve (**a**) and for the desorption peak during the ramp (**b**). It should be noted that the measured blank values have been subtracted for both cases

Figure 6b shows more clearly the increased adsorption at increased pressure, also at 300 °C. It should be noted that even though the NH_3 adsorption increases with the increasing pressure, the steady-state NO_x reduction was found to be independent of the pressure, and hence does not affect the SCR reaction, as will be further discussed during the kinetic modeling.

Figure 6a shows that by increasing the pressure 3.8 times (from 1.2 to 4.5 bar), the amount of NH_3 stored on the catalyst increases by 36% at a temperature of 150 °C. Bank et al. [34] reported for a washcoated monolith that the integral ammonia storage for a 100 cpsi vanadium-based SCR catalyst increased by approximately 70% by changing the pressure from 1 to 2 bar at 215 °C. The reason for the difference between the results reported by Bank et al., and the results obtained here is not clear, but may be related to the catalyst composition which was not disclosed in their study. Furthermore, Bank et al. [34] did not report if blank experiments were performed and subtracted, which is an important issue due to the increased mass of gas contained within the setup at increased pressure. For instance, if the blank is not subtracted, the adsorption at 150 °C increases by 46% instead of 35% when the pressure is increased by a factor 4. The blank experiments depend on the dynamics of the experimental facility, and for larger facilities, for instance using monoliths such as that used by Bank et al. [34], the effect of the blank experiment is expected to increase.

3.2.1 Modeling of the Transient Adsorption/Desorption Experiments

A transient model was set up in order to obtain the kinetics describing the adsorption-desorption processes. The gas phase concentration of NH_3 was modeled similarly to Lietti et al. [46] as an isothermal plug flow reactor, which was simplified in this study as CSTRs in series. Diffusion limitations and axial dispersion were estimated to be negligible as shown in the online supplementary material. The gas phase concentration and the surface coverage of NH_3 are therefore given by Eqs. (7) and (8).

$$\frac{dC_N}{dt} = \frac{v_0}{\varepsilon \cdot V_N}\cdot\left(C_{N-1}-C_N\right) + \left(r_{d,N}-r_{a,N}\right)\cdot\frac{1-\varepsilon}{\varepsilon}\cdot\Omega' \tag{7}$$

$$\frac{d\theta_N}{dt} = r_{a,N}-r_{d,N} \tag{8}$$

Here, N is the CSTR number, C_N is the NH_3 concentration out of the N^{th} CSTR, $C_{N\text{-}1}$ is the inlet concentration of NH_3, v_0 is the volumetric flow rate, V_N is the volume of the N^{th} CSTR, ε is the interparticle porosity of the reactor volume, Ω' is the NH_3 adsorption capacity (mol/m^3 particles), the density of the particles are 1236 kg/m^3 particles, θ_N is the surface coverage of NH_3, and $r_{a,\ N}$ and $r_{d,\ N}$ are the rate of adsorption and the rate of desorption, respectively. The rate of adsorption and desorption is given by Eq. (9) and Eq. (10), respectively.

$$r_{a,N} = k_a^0\cdot\exp\left(\frac{-E_a}{R\cdot T}\right)\cdot C_N\cdot\left(1-\theta_N\right) \tag{9}$$

$$r_{d,N} = k_d^0\cdot\exp\left(\frac{-E_d^0\cdot\left(1-\alpha\cdot\theta_N\right)}{R\cdot T}\right)\cdot\theta_N \tag{10}$$

Here, k_a^0 and E_a are the pre-exponential factor and the activation energy of the adsorption process, and k_d^0 and E_d^0 are the pre-exponential factor and the activation energy for the desorption process. α is a parameter in the Temkin isotherm.

The Temkin isotherm was reported by Lietti et al. [46] to provide a better fit compared to a regular Langmuir isotherm ($\alpha = 0$). A non-zero value of alpha induces a linear decrease in activation energy for the desorption process as the surface of the catalyst is filled by the adsorbate ($\theta \rightarrow 1$). Lietti et al. [46] found that the rate of adsorption was well represented by a non-activated ($E_a = 0$) process in line with the adsorption of an alkaline specie, such as NH_3, on the acidic surface cites of the catalyst, which will also be used in this study.

3.3 Transient Model Fitting

The unknown adsorption and desorption kinetic parameters, i.e., k_a^0, k_d^0, E_d^0, α, and Ω’, were fitted by the use of MATLAB’s® function “fmincon” using 30 CSTRs in series. According to Levenspiel [47], the number of CSTRs in series that should be used to approximate the flow profile in a fixed bed is given by Eq. (11)

$$N_{\mathrm{tanks}} = n_{\mathrm{particles}} \tag{11}$$

With a bed height of 12 mm and a particle diameter of 150–300 μm, this results in 40–80 tanks in series. Thirty CSTRs in series were initially chosen to ensure fast simulation, and the final fitting was verified against a run with 80 tanks in series which did not change the fitting results. The fitting procedure minimizes the function given by Eq. (12)

$$F(x) = \sum \left(\frac{|y_{\mathrm{meas}} - y_{\mathrm{model}}|}{y_{\mathrm{meas}}} \right) \tag{12}$$

in which y_{meas} and y_{model} are vectors containing the measured and modeled gas phase NH_3 concentration as a function of time. The blank experiments were difficult to subtract as a vector from the actual experiment, because the time signals do not fully overlay each other, and so it was decided to only fit the NH_3 peak during the ramp of temperature, during which the background was negligible (< 3 ppm NH_3).

The NH_3 capacity of the catalyst (Ω’) was calculated based on the data shown in Fig. 6a, from which it was found that the NH_3 capacity was highest at the lowest temperature (150 °C) and the highest pressure (4.5 bar) tested. Therefore, the total NH_3 adsorption capacity was calculated based on the measured total NH_3 adsorption at 150 °C and 4.5 bar to Ω’ = 228 mol NH_3/m^3 particle. It is thus assumed that the surface of the catalyst is completely filled with NH_3 ($\theta = 1$) at a pressure of 4.5 bar and at a temperature of 150 °C. In case the model predicts a non-saturated surface, a new NH_3 capacity should be calculated and a new fitting performed, hence the calculation would be iterative. As shown later, the surface coverage is found to be close to 1 (0.98). The NH_3 capacity reported by Lietti et al. [46] was 270 mol NH_3/m^3 reactor for a similar ternary 1.47 wt% V_2O_5–9 wt% WO_3-TiO_2 catalyst. As a comparison, the NH_3 capacity found in this study in the same units gives 372 mol NH_3/m^3 reactor based upon the bed porosity, as shown in Eq. (14). The bed porosity was calculated under the assumption of spherical particles based on the empirical formula presented by Pushnov [48] and shown in Eq. (13). Pushnov reported an average deviation of the formula of ± 5.26%.

$$\varepsilon = \frac{1}{\left(D_{\mathrm{reactor}}/d_{\mathrm{particle}}\right)^2} + 0.375 = 0.38 \tag{13}$$

$$\Omega = \Omega' \cdot \frac{1-\varepsilon}{\varepsilon} = 372 \frac{\mathrm{mol}}{m^3\ \mathrm{reactor}} \tag{14}$$

The calculated NH_3 capacity in the case of the pressurized experiments reported here is, therefore, higher than the one reported by Lietti et al. [46]. This is possibly due to the increased pressure used in this work and the fact that the catalysts are different. Lietti et al. [46] also reported the NH_3 capacity for a binary catalyst (V_2O_5-TiO_2), 209 mol/m^3 reactor, and explained the difference due to changes in surface area, i.e., 46 m^2/g_{cat} for the binary catalyst vs. 80 m^2/g_{cat} for the ternary catalyst. For the catalyst used in this study, a similar catalyst surface area as that for the ternary catalyst was found by N_2 adsorption calculations (BET method). The difference in NH_3 capacity can therefore not be explained by different surface areas.

With the NH_3 capacity fixed at 228 mol NH_3/m^3 particle (372 mol NH_3/m^3 reactor), the four last fitting parameters (k_a^0, k_d^0, E_d^0, and α) were fitted using 30 CSTRs in series, only fitting the NH_3 peaks, however, using the combined data with all pressures and temperatures. Based on different initial guesses, it was found that the model was able to find different parameter values that fitted the data equally well. Therefore, the quality of an individual fit was evaluated based on how well the NH_3 adsorption and desorption kinetics were able to predict the steady-state NO conversion presented earlier. It was found that the adsorption constant (k_a^0) should be large in order to predict a correct surface coverage of the catalyst, which also was able to predict the observed NO_x reduction during steady-state SCR. The only solution that was found to both fit the NH_3 TPD experiments and the steady-state SCR experiments is shown in Table 1 in which the values reported in the article by Lietti et al. [46] are also shown for comparison.

Most of the fitted values in this study are close to those reported by Lietti et al. [46], with the main difference being the rate of adsorption, which is more than ten times larger than that reported by Lietti et al. The increased rate of adsorption could be related to a more acidic catalyst, which is also in line with the higher NH_3 capacity. It was noted that a similar kinetic constant was found across the different adsorption temperatures, again indicating that the pressure does not affect the

Table 1 The fitted adsorption-desorption kinetic parameters including the parameters reported by Lietti et al. [46] for a ternary 1.47 wt% $V_2O_5/WO_3/TiO_2$ catalyst. Ω is in this study calculated based upon the amount of NH_3 adsorbed at 150 °C and 4.5 bar. E_a is assumed to be zero in both studies

Parameters Units	k_a^0 $m^3/(mol\cdot s)$	E_a kJ/mol	k_d^0 1/s	E_d^0 kJ/mol	α –	Ω mol/m^3 reactor
This study	6.8	0	$11\cdot10^5$	92.8	0.299	372
Lietti et al. [46]	0.487	0	$3\cdot10^5$	95.8	0.405	270

kinetics. A plot of how well the model predicts the measured data is shown in Figs. 7 and 8 for 1.2 bar and 4.5 bar, respectively. In the online supplementary material, a graph for each pressure (1.2 bar, 2.4 bar, 3.6 bar, and 4.5 bar) is shown together with a zoom of the NH_3 peaks.

From Fig. 7 (and the online supplementary material), it is observed that the model does not predict the desorption peak at 300 °C and 1.2 bar that well since most of the NH_3 is predicted to desorb during the 1-hour flush. At 4.5 bar (Fig. 8); however, the high-temperature peak at 300 °C is well fitted. Furthermore, from Fig. 8, it is observed that at a temperature of 150 °C and 4.5 bar, the model predicts a surface coverage of 0.98 which is close to 1, and so the fixed NH_3 adsorption capacity (Ω) of 372 mol NH_3/m^3 reactor is correct.

3.4 Modeling the Steady-State SCR Experiments Using NH_3 TPD Kinetics

The fitted NH_3 adsorption and desorption kinetics (see Table 1) were used to model the steady-state SCR experiments shown in Fig. 3. The steady-state gas phase concentration of NH_3 and NO calculated for an isothermal plug flow reactor can be written as given by Eq. (15) and Eq. (16), respectively.

$$\frac{dC_{NH_3}}{dW} = (r_d - r_a)\cdot\frac{\Omega\cdot\varepsilon}{v_0\cdot\rho\cdot(1-\varepsilon)} \tag{15}$$

$$\frac{dC_{NO}}{dW} = -r_{NO}\cdot\frac{\Omega\cdot\varepsilon}{v_0\cdot\rho\cdot(1-\varepsilon)} \tag{16}$$

In which the rate of NO reduction is given by Eq. (17) [46].

$$r_{NO} = k_{NO}\cdot C_{NO}\cdot\theta^*_{NH_3}\cdot\left(1-\exp\left(\frac{-\theta_{NH_3}}{\theta^*_{NH_3}}\right)\right) \tag{17}$$

The rate given by Eq. (17) takes into account that only a certain fraction of the sites ($\theta^*_{NH_3}$) are active in the SCR reaction. These active sites are filled up at a lower partial pressure of NH_3 than the total number of sites. For example, at a total coverage of 0.5, and with $\theta^*_{NH3} = 0.14$, as will be shown later, the fraction of covered active sites (θ^*_{NH3}) is 97%. The fraction of active sites is a constant that is fitted to the experimental data within a range of 0 to 1. The NO rate constant is assumed to follow a regular Arrhenius expression written in modified form as shown in Eq. (18).

$$k(T) = k(T_{ref})\cdot\exp\left(\frac{-E_{A,NO}}{R}\cdot\left(\frac{1}{T}-\frac{1}{T_{ref}}\right)\right) \tag{18}$$

When the Arrhenius equation is written in the form shown in Eq. (18), in which $k(T_{ref})$ and $E_{A,NO}$ are fitted, the parameters correlates less [49]. T_{ref} was chosen as 230 °C.

The steady-state surface coverage of NH_3 is now also a function of the NO reaction rate due to the equimolar consumption of NH_3 on the surface of the catalyst by NO, as given by Eq. (19).

$$\frac{d\theta_{NH3}}{dt} = 0 = r_a - r_d - r_{NO} \tag{19}$$

As shown in the online supplementary material, the effectiveness factor is above 0.9 for all pressures and for temperatures below 380 °C, and hence, diffusion limitations were not taken into account. Furthermore, the axial and radial dispersion is also calculated in the online supplementary material, showing that the assumption of plug flow is valid.

The three remaining unknown SCR-related parameters, i.e., $k(T_{ref})$, $E_{A,NO}$, and $\theta^*_{NH_3}$, were fitted to the steady-state SCR data shown in Fig. 3, using MATLAB's function "lsqcurvefit" which minimizes on the residual sum of squares (RSS). The fitted parameters are shown in Table 2 together with the parameters fitted by Lietti et al. [46] at atmospheric pressure.

The fitted kinetics, as shown in Table 2, are similar to those reported by Lietti et al. [46], and similar activation energies can be found for the SCR reaction in the literature, e.g., 55 kJ/mol [36] and 67 kJ/mol [50]; however, higher activation energies are also reported, e.g., 80 kJ/mol [51] and 94 kJ/mol [42]. Furthermore, Table 2 shows that the estimated fraction of active sites is low for both this study ($\theta^*_{NH_3} = 0.14$) and the study by Lietti et al. [46] ($\theta^*_{NH_3} = 0.12$). The low fraction of active sites means that the rate of NO disappearance will quickly be independent of the total amount of NH_3 adsorbed on the surface of the catalyst. This indicates that the active sites of the catalyst are easily covered by NH_3 and that the increased adsorption observed at increased pressure adsorbs

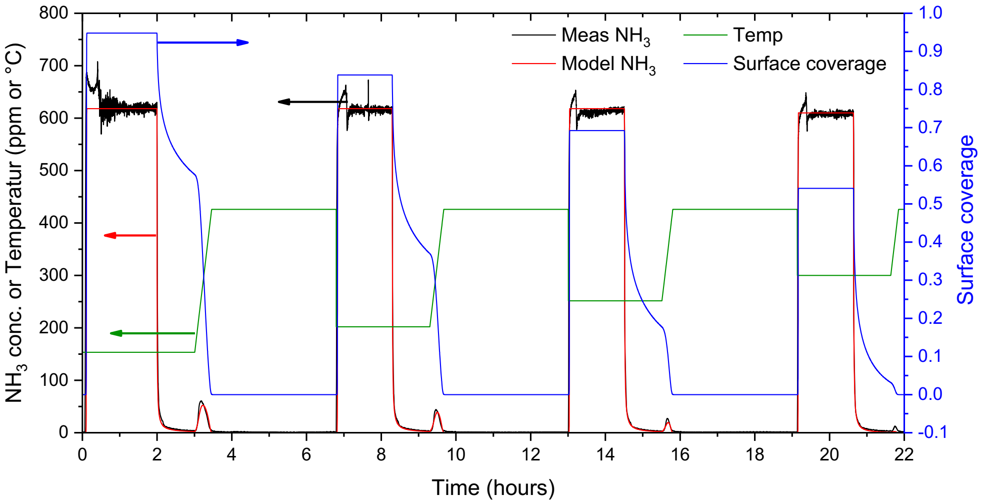

Fig. 7 Measured and predicted NH_3 adsorption and desorption at 1.2 bar, using an NH_3 concentration of 610 ppm, at four different temperatures (150, 200, 250, and 300 °C). The model is based on the fitted parameters shown in Table 1. A zoom of the desorption peeks can be found in the online supplementary material

on non-active sites, most likely on the TiO_2 support and to some extent the WO_3 promoter. Titania is known to adsorb NH_3 without having any activity in the SCR reaction, while tungsten on the other hand does exhibit SCR activity; however, the activity is in the order of 10 times below that of vanadium [46]. It is therefore expected that Ti and W mainly act as a reservoir for the NH_3 storage and that the active sites for the SCR reaction correlate to the surface coverage of vanadium as also proposed by Lietti et al. [46]. They measured the surface coverage of vanadium (θ_v) for a ternary catalyst to be $\theta^*_{NH_3} = 0.12$ *vs*. $\theta_v = 0.12$ and for a binary catalyst $\theta^*_{NH_3} = 0.08$ *vs*. $\theta_v = 0.21$ and explained that the active sites were expected to be V-OH and V=O sites as also proposed by Dumesic et al. [52]. The reservoir adsorbed NH_3 can then redistribute either through desorption-adsorption processes or through diffusion on the surface of the catalyst, which could affect the transient behavior of the catalytic system. This also explains why the increased NH_3 storage on the surface of the catalyst at increased pressure (see Fig. 6) does not result in an increased NO_x reduction since the active sites are already covered with NH_3.

3.4.1 Simulations Using the Fitted Temkin Kinetics

An experiment with a constant flow rate of 600 NmL/min containing 10% O_2, 8% H_2O, 600 ppm NO_x, and ANR = 0.8 in N_2 was performed, and the pressure was changed from 1.4 to 4.4 bar, this time with the residence time as a function of the pressure, i.e., using a flow of 600 NmL/min at all pressures. All four experiments were simulated using the Temkin isotherm, using the parameters given in Table 1 and Table 2 to test how well the model fit another set of experimental data. The results are shown in Fig. 9.

Figure 9 shows that at temperatures below 300 °C, the model predicts the experimental data well. At this low conversion of NO_x, and low temperature, the NO reduction rate is not dependent on the NH_3 concentration, i.e., the active sites $\left(\theta^*_{NH_3}\right)$ are fully covered and the model relies on the NO

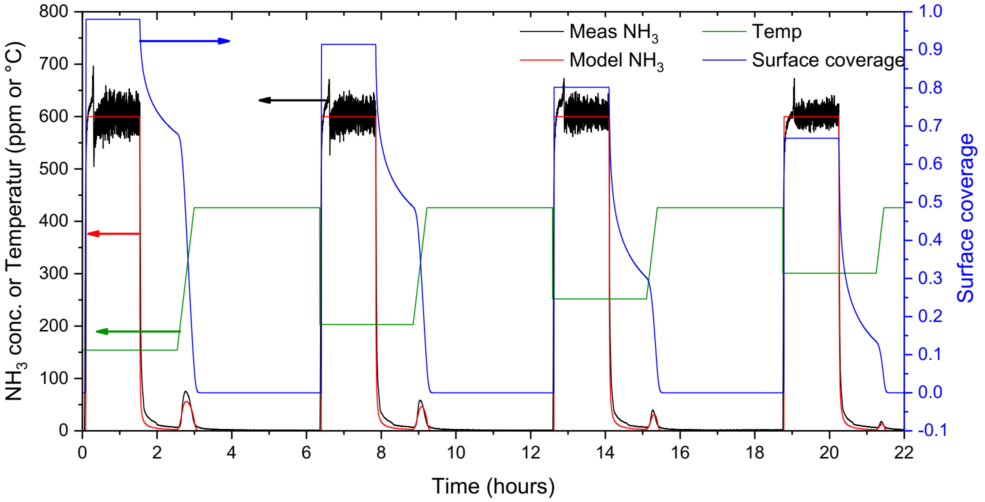

Fig. 8 Measured and predicted NH_3 adsorption and desorption at 4.5 bar, using an NH_3 concentration of 600 ppm, at four different temperatures (150, 200, 250, and 300 °C). The model is based on the fitted parameters shown in Table 1. A zoom of the desorption peeks can be found in the online supplementary material

Table 2 The fitted SCR parameters using the Temkin NH_3 adsorption and desorption parameters given in Table 1. The rate fitted by Lietti et al. [46] is based on a regular Arrhenius expression, the displayed rate constant is calculated based on the reported activation energy (59.4 kJ/mol) and pre-exponential factor ($7.19 \cdot 10^5$ m^3/s/mol)

Parameters	This study	Lietti et al. [46]
k(230 °C) [m^3/mol/s]	2.21	0.48
$E_{A,NO}$ [kJ/mol]	64.6	59.4
$\theta^*_{NH_3}$	0.141	0.121

kinetics, which was fitted for the similar steady-state experiments and hence should predict the data. At temperatures above 300 °C, the NH_3 available for the SCR reaction starts to become limiting, i.e., $\left[\theta^*_{NH_3}\cdot\left(1-\exp\left(\frac{-\theta_{NH_3}}{\theta^*_{NH_3}}\right)\right) < \theta^*_{NH_3}\right]$ and the NO_x conversion becomes more and more dependent on the NH_3 coverage, which was fitted to the separate ammonia TPD experiments. At 1.2 bar, the fitted Temkin isotherm was unable to fit the observed NH_3 desorption profile at an adsorption temperature of 300 °C (Fig. 7), and therefore, at steady-state NO_x reduction, this also becomes visible, due to a predicted too low overall NH_3 coverage and therefore also a too low coverage on the active sites. As the pressure increases, the Temkin isotherm was observed to predict the NH_3 coverage better, and as shown in Fig. 9, this is also the case in steady state NO_x reduction, as expected.

3.5 Full Monolith Experiment

SCR experiments were carried out using a V-SCR catalyst (~1 wt% V_2O_5), in the form of a monolith with an open inlet area of 223 mm^2 (see Fig. 2b). The NO_x reduction measured across the monolith as a function of temperature for the two pressures and two ANRs is shown in Fig. 10.

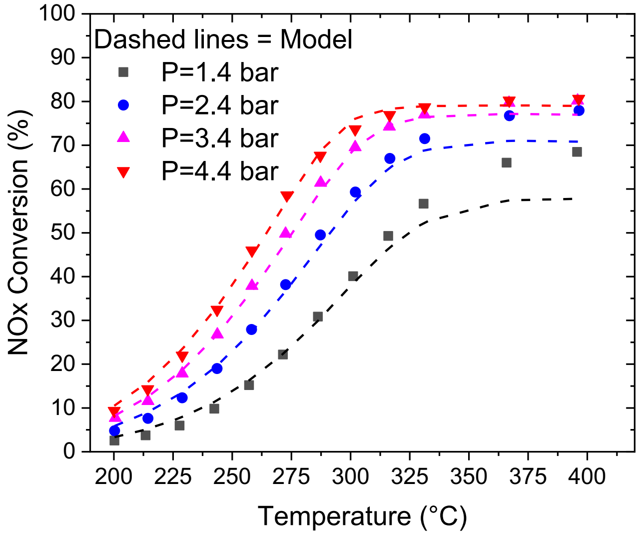

Fig. 9 Packed bed steady-state SCR experiment using 20.5 mg (~1 wt% V_2O_5) V-SCR catalyst and a total volumetric flow rate of 600 NmL/min containing 10% O_2, 8% H_2O, 600 ppm NO_x, and ANR = 0.8 in N_2 and changing the pressure without changing the total flow. Dashed lines are based on the Temkin parameters shown in Table 1 and Table 2

Figure 10 shows that at the low temperature of 200 °C, similar NO_x conversions are observed independently of the pressure when the residence time is constant. As the temperature is increased, a lower NO_x conversion is observed for the 3.1 bar experiment, which was not observed in the packed bed reactor experiments. The lower NO_x conversion at elevated pressures becomes visible around 250 °C and more pronounced as the temperature is increased. At a temperature of approximately 250 °C, the SCR reaction across a monolith starts to become influenced by external and internal diffusion limitations, and as the temperature is increased, these limitations become more pronounced [24]. The increased diffusion limitations at increased pressure are linked to the inverse proportionality between pressure and the binary diffusion coefficient which will limit the SCR reaction. The same trends were reported by Kröcher et al. [35] for a similar monolith experiment.

To simulate the monolith experiments, including the increased diffusion limitations observed at increased pressure, a single-channel monolith model developed by Olsen [53] was used. The model is a 1D-1D single channel monolith model, which calculates the concentration profiles of NH_3 and NO both in the radial direction within the catalytic wall and in the axial direction. The model was developed to simulate the deactivation of SCR monoliths caused by KCl deposition; however, in this study, only the SCR reaction part of the model is used. The model is based on Eley-Rideal kinetics (see Eq. (6)), and therefore, the steady-state SCR experiments from the packed bed reactor (Fig. 3) were re-fitted under the assumption of a plug flow reactor and following the Eley-Rideal mechanism as shown in Eq. (20).

$$\frac{dC_{NO}}{dW} = \frac{k'_{NO}\cdot C_{NO}}{v_0}\cdot\frac{K_{NH3}\cdot C_{NH3}}{1+K_{NH3}\cdot C_{NH3}} \tag{20}$$

Both the NO rate constant and the NH_3 adsorption equilibrium constant were assumed to follow an Arrhenius equation. The fitted parameters are shown in Table 3, and in Fig. 11, a plot similar to Fig. 9 is shown, but now also displaying how well the Eley-Rideal kinetics fit the experimental data.

In Table 3, the pre-exponential factor and the activation energy for the NO rate constant are shown together with the pre-exponential factor and the adsorption enthalpy of NH_3, both of which are used to calculate the rate of NO reduction in the monolith model.

When modeling reactions in a monolith, a correlation for the external mass transfer coefficient for developing laminar flow is often applied, such as that proposed by Tronconi et al.

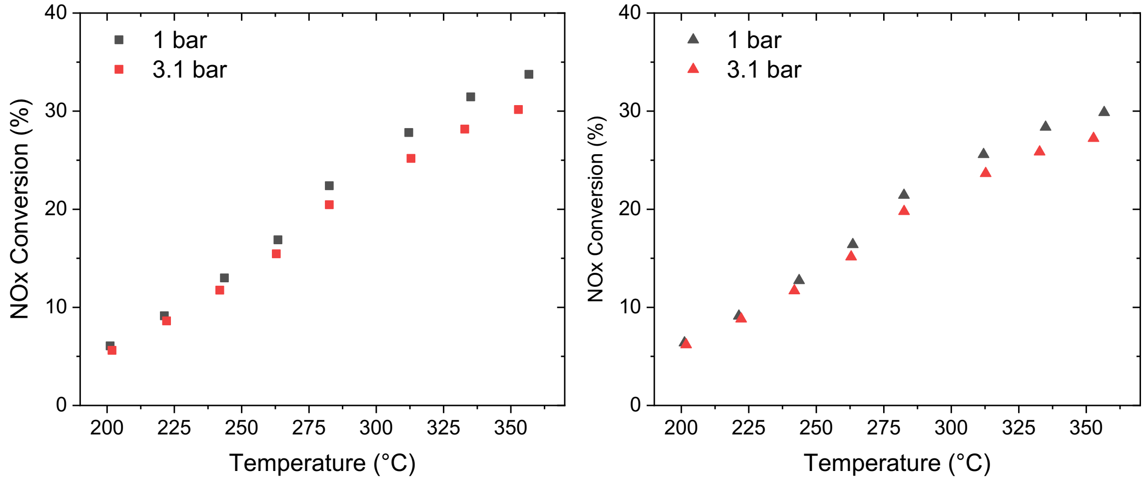

a ANR = 1.16 **b** ANR = 0.75

Fig. 10 Monolith experiments using a total volumetric flow rate of 4.9 Nm^3/h at 1 bar containing 8% O_2, 5% H_2O, 720 ppm NO_x, ANR = 1.16 (**a**), or ANR = 0.75 (**b**) in N_2. At 3.1 bar, a total volumetric flow rate of 14.5 Nm^3/h was used, and hence, the actual residence time is similar at the two pressures

[42, 55], based upon the work of Shah et al. [56] and London et al. [57] as shown in Eq. (21).

$$\mathrm{Sh} = \mathrm{Sh}_\infty + 8.827\cdot\left(1000\cdot Z^*\right)^{-0.545}\exp\left(-48.2\cdot Z^*\right) \qquad (21)$$

$$Z^* = \frac{z\cdot D_{\mathrm{AB}}}{U\cdot d_{\mathrm{h}}^2} \qquad (22)$$

Here, Sh_∞ is the asymptotic Sherwood number, which depends on the channel geometry, and Z^* is the dimensionless axial coordinate given by Eq. (22), in which z is the axial coordinate, D_{AB} is the binary diffusion coefficient, U is the linear velocity, and d_{h} is the hydraulic diameter. Equation (21) was found to give poor agreement with the experimental results, predicting a too low NO_x conversion as shown for 3.1 bar in Fig. 12. Since the powder used in the packed bed experiments was obtained from a similar monolith, this discrepancy was attributed to a too low mass transfer coefficient. It was therefore considered that the assumption of a developing laminar flow was not applicable to this experiment using a short monolith (10 cm) and a high flow rate. The Reynolds number within the monolith channel was calculated to be approximately 1000 at 1 bar and 3000 at 3 bar. Therefore, a mean mass transfer coefficient for the channel was instead calculated based upon laminar flow in tubes, as given by Eq. (23) [47] at 1 bar. At high pressure however, this correlation, valid for laminar flow, was found to be inadequate. Since the Reynolds number is in the intermediate range between turbulent and laminar flow, a turbulent model for flow in tubes (Eq. (24) [47]) was tested. An estimate of the roughness of the catalyst

Table 3 The fitted Eley-Rideal parameters using the packed bed experimental data presented in Fig. 3 and the fitted parameters reported by Koebel and Elsener [54]. The NO rate constant and the NH_3 equilibrium constant are both assumed to follow an Arrhenius equation

Parameters	This study	Koebel and Elsener [54]
$k'_{\mathrm{NO}}(T_{230})$ [$m^3/s/kg$]	0.0588	0.014
$E_{A,\mathrm{NO}}$ [kJ/mol]	62.5	74.7
$K_{\mathrm{NH3},0}$ [Pa^{-1}]	$24.1\cdot10^{-12}$	$3\cdot10^{-12}$
$\Delta H_{\mathrm{NH3,ad}}$ [kJ/mol]	−114.6	−137

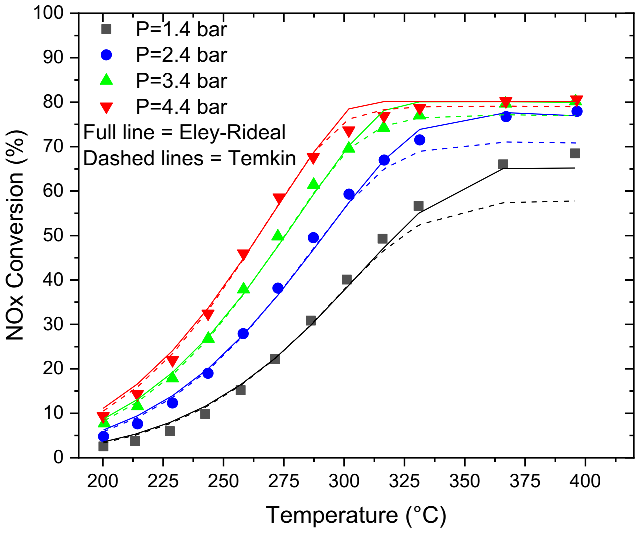

Fig. 11 Steady-state SCR experiment using 20.5 mg (~1 wt% V_2O_5) V-SCR catalyst and a total volumetric flow rate of 600 NmL/min containing 10% O_2, 8% H_2O, 600 ppm NO_x, and ANR = 0.8 in N_2 and changing the pressure without changing the flow. Dashed lines are based on the Temkin parameters shown in Table 1 and Table 2, and full lines are based on Eley-Rideal kinetics using the parameters shown in Table 3

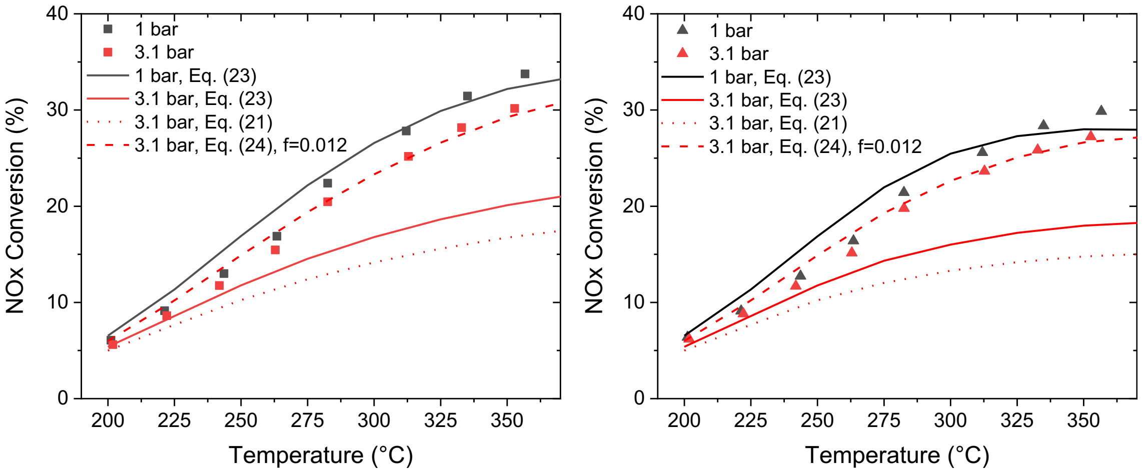

a ANR = 1.16

b ANR = 0.75

Fig. 12 The monolith experiment also is shown in Fig. 10. The model developed by Olsen et al. [53] was used to predict the experimental data, using the PBR kinetics as shown in Table 3. The external mass transfer coefficient was calculated assuming pure laminar flow at 1 bar (Eq. (23)) and as both developing laminar flow (Eq. (21)), laminar flow (Eq. (23)), and turbulent flow at 3.1 bar (Eq. (24))

channel surface of 0.03 mm was found to result in a friction factor (f) of approximately 0.012, which was calculated based upon the Churchill equations [58], which gave a good fit for the NO_x conversion.

$$\mathrm{Sh} = 1.86{\cdot}Gz^{1/3} = 1.86{\cdot}\left(\mathrm{Re}{\cdot}\mathrm{Sc}{\cdot}\frac{d_h}{L}\right)^{1/3} \tag{23}$$

$$\mathrm{Sh} = 0.5{\cdot}f{\cdot}\mathrm{Re}{\cdot}\mathrm{Sc}^{1/3} \tag{24}$$

Here, Re is the Reynolds number, Sc is the Schmidt's number, d_h is the hydraulic diameter, and L is the length of the monolith. The model prediction using these expressions for external mass transfer limitations is shown in Fig. 12.

Figure 12 shows that the use of developing laminar flow results in a large error as high as 15% points in the calculated NO_x conversion compared to the observed NO_x reduction. The more general correlations as given in Eq. (23) at a Reynolds number of 1000 (1 bar) and Eq. (24) at a Reynolds number of 3000 (3.1 bar) were found to give better agreement. The model predicts a drop in NO_x conversion when the pressure is increased due to increased diffusion limitations. Regular length, full open monoliths should be tested in a future study, to see how well mass transfer correlations for developing laminar flow predicts the external mass transfer at increased pressure when a more typical channel velocity (3–5 m/s) and length of catalyst (0.5 m) is used. From this study, it is concluded that at an increased pressure, when the residence time is kept constant, a decrease in NO_x reduction efficiency is observed, due to increasing external and internal mass transfer limitations, as also discussed by Kröcher et al. [35].

It should be noted that the drop in NO_x reduction is only observed because the residence time is kept constant with variations in the pressure. If an SCR reactor was installed on a ship, the residence time would increase with increasing pressure, and the total effect of increasing pressure becomes positive. Kröcher et al. [35] measured that to achieve 70% NO_x reduction at 350 °C and having an NH_3 slip of 10 ppm, the volume of a 87 cpsi catalyst could be reduced from 100% at 1 bar, to 80% at 2 bar and 70% at 4 bar, which shows that in total a positive effect of pressure is obtained. If no diffusion limitations had been present, the catalyst volume could have been reduced to 50% and 25% at 2 and 4 bar, respectively.

4 Conclusion

The following conclusions can be drawn from this study of SCR of NO_x at pressures up to 5 bar for a ~ 1 wt% V_2O_5/10 wt% WO_3/TiO_2 catalyst.

- The measured NO_x conversion was independent of the pressure in the range 1.2–4.8 bar over a packed bed reactor with catalyst particles in the sieve range 150–300 μm with no diffusion limitations, when the residence time was kept constant. This shows that the kinetics are independent of pressure up to 5 bar.
- A transient model for NH_3 adsorption/desorption on the catalyst based on a Temkin isotherm was fitted to the experimental data. The data indicates that only a certain fraction of the total sites onto which NH_3 adsorbs are truly active in the SCR reaction. This fraction was found to be about 14%. It was further found that these sites fill up at lower NH_3 partial pressure compared to all sites.
- The adsorption of NH_3 on the catalyst was found to increase with increasing pressure and decrease with

increasing temperature. The increased adsorption at increased pressure was found to be on non-active sites, and the rate of NO_x reduction was therefore not promoted by the increased adsorption of NH_3.

- Experiments using a monolith showed that at an increased pressure of 3.1 bar, keeping the gas residence time constant relative to at 1 bar, a decrease in NO_x reduction was observed at temperatures above 250 °C. This decrease was attributed to a decrease in the binary diffusion coefficient, which is inversely proportional to the pressure. The drop in NO_x conversion was confirmed by a 1D-1D model.
- Estimation of the external mass transfer coefficient using correlations for developing laminar flow lead to a poor agreement with the experimental data, and instead, a correlation for turbulent flow was required, probably due to the high channel velocity (10–13 m/s) used in this work.
- This study has shown that the intrinsic kinetics of the SCR reaction is independent on pressure, and so, kinetics determined at 1 bar can be used for the design of SCR reactors also at elevated pressures, such as upstream of the turbocharger on a two-stroke marine diesel engine. The increased pressure does affect the binary diffusion coefficient and hence increased mass transfer limitations will take effect on monolithic catalysts at temperatures above approximately 250 °C.

Acknowledgments This work is part of the Danish societal partnership, Blue INNOship, and partly funded by the Innovation Fund Denmark (IFD) under File No: 155-2014-10 and the Danish Maritime Fund. The authors gratefully acknowledge the funding support.

Compliance with Ethical Standards

The authors declare that they have no competing interests.

Abbreviations *ABS,* Ammonium bisulfate; *ANR,* Ammonia to NO_x ratio; *AS,* Ammonium sulfate; *CPSI,* Channels per square inch; *CSTR,* Continuous stirred tank reactor; *EGR,* Exhaust gas recirculation; *IMO,* International maritime organization; *LNG,* Liquid natural gas; *NECA,* NO_x emission control area; *NO_x,* Nitrogen oxides, the sum of NO and NO_2; *PBR,* Packed bed reactor; *RSS,* Residual sum of squares; *SCR,* Selective catalytic reduction; *SECA,* SO_x emission control area; *SO_x,* Sulfur oxides, the sum of SO_2, SO_3, and H_2SO_4; *V-SCR,* Vanadium-based SCR catalyst

Symbols α, Temkin kinetics parameter [−]; C_{NH3}, NH_3 concentration [mol/m^3]; $d_{particle}$, Catalyst particle diameter [m]; $D_{reactor}$, Reactor tube diameter [m]; D_{AB}, Binary diffusion coefficient [m/s^2]; d_h, Hydraulic diameter [m]; ε, Porosity [−]; E_a, Activation energy of the adsorption process of NH_3 [J/mol]; E_d^0 , Activation energy for the desorption process of NH_3 [J/mol]; f, Friction factor [−]; G_z, Graetz dimensional number [−]; k_{NO}, NO first order rate constant [1/s]; k'_{NO}, Mass based NO first order rate constant [m^3/s/kg]; k_a^0 , Pre-exponential factor of the adsorption process of NH_3 [m^3/mol/s]; k_d^0 , Pre-exponential factor for the desorption process of NH_3 [1/s]; K_{NH_3} , NH_3 adsorption equilibrium constant [m^3/mol]; $k(T_{ref})$, Reaction rate constant calculate at the temperature T_{ref}; L, Length of catalyst [m]; Ω', NH_3 adsorption capacity (mol/m^3 particles); $\Omega = \Omega' \cdot \frac{1-\varepsilon}{\varepsilon}$, NH_3 adsorption capacity (mol/m^3 reactor); $P_{reactor}$, Reactor pressure [Pa]; Q_0, Volumetric flow rate (normal (0 °C, 1 atm)) [Nm^3/s]; r_a, Rate of adsorption of NH_3 [1/s]; r_d, Rate of desorption of NH_3 [1/s]; *Re,* Reynolds dimensional number [−]; ρ, Density of catalyst [kg/m^3]; r_{NO}, Rate of NO disappearance [1/s]; S_c, Schmidts dimensional number [−]; *Sh,* Sherwood dimensional number [−]; Sh_∞, Asymptotic Sherwood number [−]; θ, Surface coverage of NH_3 [−]; $\theta_{NH_3}^*$, Fraction of active sites in the SCR reaction [−]; θ_v, Surface coverage of vanadium [−]; *U,* Linear velocity [m/s]; *V,* Volume [m^3]; v_0, volumetric flow rate [m^3/s]; *W,* Weight of catalyst [kg]; y_{meas}, Vectors containing the measured gas phase mole fraction [ppm]; y_{model}, Vectors containing the modeled gas phase mole fraction [ppm]; *z,* Axial coordinate [m]; *Z**, Dimensionless axial coordinate [−]

References

1. Hallquist, Å.M., Fridell, E., Westerlund, J., Hallquist, M.: Onboard measurements of nanoparticles from a SCR-equipped marine diesel engine. Environ. Sci. Technol. **47**(2), 773–780 (2013). https://doi.org/10.1021/es302712a
2. Man Diesel & Turbo, Exhaust gas emission control today and tomorrow. http://marine.man.eu/docs/librariesprovider6/technical-papers/exhaust-gas-emission-control-today-and-tomorrow.pdf?sfvrsn=22 (accessed September 10, 2015).
3. Lamas, M.I., Rodríguez, C.G.: Emissions from marine engines and NO_x reduction methods. J. Marit. Res. **9**, 77–81 (2012)
4. Briggs, J., Mccarney, J.: Field Experience of Marine SCR. CIMAC Congr (2013)
5. Niki, Y. Hirata, K. Kishi, T. Inaba, T. Takagi, M. Fukuda, T. Nagai, T. Muraoka, E.: SCR System for NO_x reduction of medium speed marine diesel engine, in: CIMAC Congress, Vol. 22 p. 12 (2010)
6. G. Lövblad, E. Fridell, Experiences from use of some techniques to reduce emissions from ships, Göteborg. http://cleantech.cnss.no/wp-content/uploads/2011/09/2006-Lovblad-and-Fridell-Experiences-from-use-of-some-techniques-to-reduce-emissions-from-ships.pdf. (2006). Accessed 16 Dec 2015
7. Magnusson, M., Fridell, E., Ingelsten, H.H.: The influence of sulfur dioxide and water on the performance of a marine SCR catalyst. Appl. Catal. B Environ. **111–112**, 20–26 (2012). https://doi.org/10.1016/j.apcatb.2011.09.010
8. Österman, C., Magnusson, M.: A systemic review of shipboard SCR installations in practice. WMU J. Marit. Aff. **12**(1), 63–85 (2013). https://doi.org/10.1007/s13437-012-0034-1
9. Lehtoranta, K., Vesala, H., Koponen, P., Korhonen, S.: Selective catalytic reduction operation with heavy fuel oil: NO_x , NH3, and particle emissions. Environ. Sci. & Technol. **49**(7), 4735–4741 (2015). https://doi.org/10.1021/es506185x
10. Det Norske Veritas (DNV), Marpol 73/78 Annex VI, (2009). http://hulpinnood.nl/wp-content/uploads/2015/03/BIJLAGE3_Marpol-annex-VI.pdf (accessed May 9, 2016)
11. IMO, The 2020 Global Sulfur Limit. http://www.imo.org/en/MediaCentre/HotTopics/GHG/Documents/FAQ_2020_English.pdf (accessed October 12, 2017)
12. IMO, Emission Control Areas designated under MARPOL Annex VI, (2018). http://www.imo.org/en/OurWork/Environment/PollutionPrevention/AirPollution/Pages/Emission-Control-Areas-(ECAs)-designated-under-regulation-13-of-MARPOL-Annex-VI-(NOx-emission-control).aspx (accessed January 12, 2019)
13. Mollenhauer, K., Tschöke, H.: Handbook of Diesel Engines. Springer Berlin Heidelberg, Berlin (2010). https://doi.org/10.1007/978-3-540-89083-6
14. Turns, S.R.: An introduction to combustion: concepts and applications. New York, NY: McGraw-Hill (2012)

15. Forzatti, P., Lietti, L.: Recent advances in DeNOxing catalysis for stationary applications. Heterog. Chem. Rev. **3**(1), 33–51 (1996)
16. Koebel, M., Elsener, M., Madia, G.: Recent advances in the development of urea-SCR for automotive applications. Sae Tech. Pap. (2001). https://doi.org/10.4271/2001-01-3625
17. P. Blakeman, K. Arnby, P. Marsh, C. Newman, G. Smedler, Optimization of an SCR catalyst system to meet EUIV heavy duty diesel legislation, SAE Tech. Pap. 2 (2008). https://doi.org/10.4271/2008-01-1542
18. Guan, B., Zhan, R., Lin, H., Huang, Z.: Review of state of the art technologies of selective catalytic reduction of NO_x from diesel engine exhaust. Appl. Therm. Eng. **66**(1-2), 395–414 (2014). https://doi.org/10.1016/j.applthermaleng.2014.02.021
19. Kröcher, O.: Aspects of catalyst development for mobile urea-SCR systems—from Vanadia-Titania catalysts to metal-exchanged zeolites. Stud. Surf. Sci. Catal. **171**, 261-289 (2007) https://doi.org/10.1016/S0167-2991(07)80210-2.
20. Man Diesel & Turbo, Tier III Two-Stroke Technology, (2012). http://marine.man.eu/docs/librariesprovider6/technical-papers/tier-iii-two-stroke-technology.pdf?sfvrsn=12 (accessed September 10, 2015)
21. IMO, IMO MEPC 66/6/15, (2014). http://www.worldshipping.org/industry-issues/environment/air-emissions/MEPC_66-6-15_-_Comments_concerning_potential_amendments_to_the_effective___.pdf (accessed November 20, 2017).
22. H. Bosch, F. Janssen, Preface, Catal. Today. 2 v. https://doi.org/10.1016/0920-5861(88)80001-4 (1988)
23. G. Centi, S. Perathoner: Chapter 1 introduction: state of the art in the development of catalytic processes for the selective catalytic reduction of NO_x into N_2. in: Stud. Surf. Sci. Catal., pp. 1–23. https://doi.org/10.1016/S0167-2991(07)80202-3. 2007
24. Gabrielsson, P., Pedersen, H.G.: Flue gas from stationary sources. In: Ertl, G., Knözinger, H., Schüth, F., Weitkamp, J. (eds.) Handb. Heterog. Catal, pp. 2345–2385. Wiley-VCH (2008) http://findit.dtu.dk/en/catalog/2342172429 (accessed March 29, 2017)
25. I. Nova, E. Tronconi: Urea-SCR Technology for deNO_x After Treatment of Diesel Exhausts, Springer. https://doi.org/10.1007/978-1-4899-8071-7 (2014)
26. Marine Fuels 2020. https://www.marinefuels2020.com/marine-fuels/background/ (accessed April 6, 2019).
27. CIMAC Working Group 8, CIMAC Guideline: Cold Corrosion in Marine Two Stroke, CIMAC Guidel. (2017) 1–36.https://cimac.com/cms/upload/Publication_Press/WG_Publications/CIMAC_WG8_Guideline_2017_Two_Stroke_Engine_Cold_Corrosion.pdf. Accessed 27 June 2018
28. Orsenigo, C., Beretta, A., Forzatti, P., Svachula, J., Tronconi, E., Bregani, F., Baldacci, A.: Theoretical and experimental study of the interaction between NO_x reduction and SO_2 oxidation over DeNOx-SCR catalysts. Catal. Today. **27**(1-2), 15–21 (1996). https://doi.org/10.1016/0920-5861(95)00168-9
29. Tronconi, E., Cavanna, A., Orsenigo, C., Forzatti, P.: Transient kinetics of SO_2 oxidation over SCR-DeNO_x monolith catalysts. Ind. Eng. Chem. Res. **38**(7), 2593–2598 (1999). https://doi.org/10.1021/ie980673e.
30. Muzio, L., Bogseth, S., Himes, R., Chien, Y.-C., Dunn-Rankin, D.: Ammonium bisulfate formation and reduced load SCR operation. Fuel. **206**, 180–189 (2017). https://doi.org/10.1016/j.fuel.2017.05.081
31. J.M. Burke, K.L. Johnson: Ammonium sulfate and bisulfate formation in air preheaters (project summary). http://nepis.epa.gov/Exe/ZyPURL.cgi?Dockey=2000TU1N.txt.1982. Accessed 21 Sept 2015
32. Matsuda, S., Kamo, T., Kato, A., Nakajima, F., Kumura, T., Kuroda, H.: Deposition of ammonium bisulfate in the selective catalytic reduction of nitrogen oxides with ammonia. Ind. Eng. Chem. Prod. Res. Dev. **21**(1), 48–52 (1982). https://doi.org/10.1021/i300005a009
33. T. Fujibayashi, S. Baba, H. Tanaka: Development of Marine SCR System for Large Two-Stroke Diesel Engines Complying with IMO NO_x Tier III. in: CIMAC Congr. (2013)
34. R. Bank, B. Buchholz, H. Harndorf, R. Rabe, U. Etzien: High-Pressure SCR at Large Diesel Engines for Reliable NO_x -Reduction and Compliance with IMO Tier III Standards, in: CIMAC Congr. 2013
35. Kröcher, O., Elsener, M., Bothien, M.-R., Dölling, W.: Pre-Turbo SCR - influence of pressure on NO_x reduction. MTZ Worldw. **75**(4), 46–51 (2014). https://doi.org/10.1007/s38313-014-0140-x
36. Rammelt, T., Torkashvand, B., Hauck, C., Böhm, J., Gläser, R., Deutschmann, O.: Nitric oxide reduction of heavy-duty diesel off-gas by NH3-SCR in front of the turbocharger. Emiss. Control Sci. Technol. **3**(4), 275–288 (2017). https://doi.org/10.1007/s40825-017-0078-y
37. K. Sandelin, D. Peitz: SCR under pressure - pre-turbocharger NO_x abatement for marine 2-stroke diesel engines, in: CIMAC Congr. (2016)
38. Schüttenhelm, W., Günther, C., Jürgens, R.: High pressure SCR for large two-stroke engines and comparison to conventional SCR high dust applications. VGB Powertech. **8**, 58–62 (2017)
39. Bird, R.B., Stewart, W.E., Lightfoot, E.N.: Transport phenomena. J. Wiley pp. xii, 905 s (2007)
40. Christensen, S.R., Hansen, B.B., Johansen, K., Pedersen, K.H., Thøgersen, J.R., Jensen, A.D.: SO_2 oxidation across marine V_2O_5-WO_3-TiO_2 SCR catalysts: a study at elevated pressure for preturbine SCR configuration. Emiss. Control Sci. Technol. **4**(4), 289–299 (2018). https://doi.org/10.1007/s40825-018-0092-8
41. Koebel, M., Madia, G., Elsener, M.: Selective catalytic reduction of NO and NO_2 at low temperatures. Catal. Today. **73**(3-4), 239–247 (2002). https://doi.org/10.1016/S0920-5861(02)00006-8
42. Tronconi, E., Forzatti, P., Gomez Martin, J.P., Mallogi, S.: Selective catalytic removal of NO_x: a mathematical model for design of catalyst and reactor. Chem. Eng. Sci. **47**(9-11), 2401–2406 (1992). https://doi.org/10.1016/0009-2509(92)87067-Z
43. Nova, I., Lietti, L., Beretta, A., Forzatti, P.: Study of the sintering of a deNOx commercial catalyst. Stud. Surf. Sci. Catal. **139**, 149–156 (2001). https://doi.org/10.1016/S0167-2991(01)80192-0
44. Dumesic, J.A., Topsøe, N.-Y., Topsøe, H., Chen, Y., Slabiak, T.: Kinetics of selective catalytic reduction of nitric oxide by Ammonia over Vanadia/Titania. J. Catal. **163**(2), 409–417 (1996). https://doi.org/10.1006/jcat.1996.0342
45. Tsukahara, H., Ishida, T., Mayumi, M.: Gas-phase oxidation of nitric oxide: chemical kinetics and rate constant. Nitric Oxide. **3**(3), 191–198 (1999). https://doi.org/10.1006/niox.1999.0232
46. Lietti, L., Nova, I., Camurri, S., Tronconi, E., Forzatti, P.: Dynamics of the SCR-DeNO_x reaction by the transient-response method. AIChE J. **43**(10), 2559–2570 (1997). https://doi.org/10.1002/aic.690431017
47. Levenspiel, O.: The chemical reactor omnibook, Distributed by OSU Book Stores, (1989)
48. Pushnov, A.S.: Calculation of average bed porosity. Chem. Pet. Eng. **42**(1-2), 14–17 (2006). https://doi.org/10.1007/s10556-006-0045-x
49. Rawlings, J.B., Ekerdt, J.G.: Chemical reactor analysis and design fundamentals, 2. Edition, Madison, Wis.: Nob Hill Pub (2002)
50. Forzatti, P., Nova, I., Beretta, A.: Catalytic properties in deNO_x and SO_2–SO_3 reactions. Catal. Today. **56**(4), 431–441 (2000). https://doi.org/10.1016/S0920-5861(99)00302-8
51. Beeckman, J.W., Hegedus, L.L.: Design of monolith catalysts for power plant NO_x emission control. Ind. Eng. Chem. Res. **30**(5), 969–978 (1991). https://doi.org/10.1021/ie00053a020
52. J.A. Dumesic, N.-Y. Topsoe, T. Slabiak, P. Morsing, B.S. Clausen, E. Törqvist, H. Topsoe: Microiunetic analysis of the selective

catalytic reduction (SCR) of nitric oxide over Vanadia/Titania-based Catalysts, in. pp. 1325–1337. https://doi.org/10.1016/S0167-2991(08)64454-7 (1993)

53. Olsen, B.K., Castellino, F., Jensen, A.D.: Modeling deactivation of catalysts for selective catalytic reduction of NO_x by KCl aerosols. Ind. Eng. Chem. Res. **56**(45), 13020–13033 (2017). https://doi.org/10.1021/acs.iecr.7b01239.
54. Koebel, M., Elsener, M.: Selective catalytic reduction of NO over commercial DeNOx catalysts: comparison of the measured and calculated performance. Ind. Eng. Chem. Res. **37**(2), 327–335 (1998). https://doi.org/10.1021/ie970569h.
55. Tronconi, E., Forzatti, P.: Adequacy of lumped parameter models for SCR reactors with monolith structure. AICHE J. **38**(2), 201–210 (1992). https://doi.org/10.1002/aic.690380205
56. Shah, R.K., London, A.L.: Laminar flow forced convection in ducts. New York: Academic Press (1978)
57. Tratz, H., Grigull, U.: Thermischer Einlauf in Ausgebildeter Laminarer Rohrströmung. Int. J. Heat Mass Transf. **8**, 669–678 (1965)
58. Clement, K.H. Fangel, P. Jensen, A.D. Thomsen, K.: Kemiske enhedsoperationer, Polyteknisk Forlag. (2004)